^<13>N-ammonia positron emission tomography-derived endocardial strain for the assessment of ischemia using feature-tracking in high-resolution cine imaging

Kawakubo, Masateru
Department of Health Sciences, Faculty of Medical Sciences, Kyushu University

Nagao, Michinobu
Department of Diagnostic Imaging & Nuclear Medicine, Tokyo Women's Medical University

Yamamoto, Atsushi
Department of Diagnostic Imaging & Nuclear Medicine, Tokyo Women's Medical University

Nakao, Risako
Department of Cardiology, Tokyo Women's Medical University

他

出版情報：Journal of nuclear cardiology, 2021-06-11. Springer
バージョン：
権利関係：

^{13}N-ammonia positron emission tomography-derived endocardial strain for the assessment of ischemia using feature-tracking in high-resolution cine imaging

Masateru Kawakubo[a], PhD, *Michinobu Nagao[b], MD, Atsushi Yamamoto[b], MD, Risako Nakao[c], MD, Yuka Matsuo[b], MD, Kenji Fukushim[d], MD, Eri Watanabe[c],MD, Akiko Sakai[c], MD, Masayuki Sasaki[a], MD, and Shuji Sakai[b], MD

a. Department of Health Sciences, Faculty of Medical Sciences, Kyushu University, Fukuoka, Japan
b. Department of Diagnostic Imaging & Nuclear Medicine, Tokyo Women's Medical University, Tokyo, Japan
c. Department of Cardiology, Tokyo Women's Medical University, Tokyo, Japan
d. Department of Nuclear Medicine, Saitama Medical University, Saitama, Japan

***Corresponding author**: Michinobu Nagao, MD, Associate Professor
Department of Diagnostic Imaging & Nuclear Medicine, Tokyo Women's Medical University
8-1 Kawada-cho, Shinjuku-ku, Tokyo 162-8666, Japan
Tel: +81-3-3353-8111
Fax: +81-3-5269-9247
E-mail: nagao.michinobu@twmu.ac.jp

Disclosure

Masateru Kawakubo has no conflicts of interest to declare.

Michinobu Nagao has no conflicts of interest to declare.

Atsushi Yamamoto has no conflicts of interest to declare.

Risako Nakao has no conflicts of interest to declare.

Yuka Matsuo has no conflicts of interest to declare.

Kenji Fukushim has no conflicts of interest to declare.

Eri Watanabe has no conflicts of interest to declare.

Akiko Sakai has no conflicts of interest to declare.

Masayuki Sasaki has no conflicts of interest to declare.

Shuji Sakai has no conflicts of interest to declare.

Funding: This work was supported by JSPS KAKENHI, Grant Numbers JP20K16729 and JP16K19860.

Abstract

Background: Assessing endocardial strain using a single ^{13}N-ammonia positron emission tomography (PET) scan would be clinically useful, given the association between ischemia and myocardial deformation. However, no software has been developed for strain analysis using PET. We evaluated the clinical potential of feature tracking-derived strain values measured using PET, based on associations with the myocardial flow reserve (MFR).

Methods and Results: This retrospective study included 95 coronary artery disease patients who underwent myocardial ^{13}N-ammonia PET. Semi-automatic measurements were made using a feature-tracking technique during myocardial cine imaging, and values were calculated using a 16-segment model. Adenosine-stressed global circumferential strain (CS) and global longitudinal strain (LS) values were compared with global MFR values. Stressed and resting global strain values were also compared. Global strain values were significantly lower in 39 patients with abnormal MFRs [<2.0] than in 56 patients with normal MFRs [≥2.0]. The global CS values in the stressed state were significantly decreased than the resting state values in patients with abnormal MFRs.

Conclusions: This study applied endocardial feature-tracking to ^{13}N-ammonia PET, and the results suggested that blood flow and myocardial motility could be clinically assessed in ischemic patients using a single PET scan.

Keywords: ^{13}N-ammonia PET, left ventricular strain, high-resolution cine imaging, feature-tracking, myocardial ischemia

Abbreviations

PET: positron emission tomography

ECG: electrocardiography

CS: circumferential strain

LS: longitudinal strain

MFR: myocardial flow reserve

LV: left ventricular

EF: ejection fraction

RCA: right coronary artery

LAD: left anterior descending artery

LCx: left circumflex coronary artery

Introduction

Electrocardiography (ECG)-gated ^{13}N-ammonia positron emission tomography (PET) provides high temporal and spatial resolution and is superior to single-photon emission computed tomography for detecting myocardial ischemia. ^{13}N-ammonia PET is essential for assessing myocardial blood flow at rest, hyperemia-induced adenosine stress, and coronary flow reserve. Patients with myocardial ischemia can be assessed using the PET-derived summed stress score, summed rest score, summed difference score, myocardial flow reserve (MFR), and stressed:resting ratio of the myocardial blood flow (*1-5*). Contours of the myocardium, including the left ventricular (LV) papillary muscle, can also be clearly visualized using a PET-computed tomography scanner equipped with time-of-flight correction (*6*). Recent technical improvements in time-of-flight systems may improve the high spatial resolution of ^{13}N-ammonia PET, although this modality is currently limited to measuring LV volume, mass, and ejection fraction (EF) (*7*). Wall thickening analysis can be performed based on quantitative gated single-photon emission computed tomography, although frequent misregistration occurs in the extraction of the myocardial contours when this method is applied to PET. Furthermore, high background noise in single-photon emission computed tomography images make them unsuitable for feature-tracking analysis. Thus, no PET-dedicated regional motion analysis software has been developed, and analyses are currently based on software for single-photon emission computed tomography.

Myocardial regional strain derived from cardiac magnetic resonance is inversely associated with infarct size and LV remodeling during myocardial ischemia (*8-11*). Feature-tracking based on routine cardiac magnetic resonance cine imaging provides data from three principal vectors that describe the deformation mechanics in LV geometry: circumferential strain (CS), longitudinal strain (LS), and radial strain (*12*). Because ischemia evolves from the endocardium to the epicardium, endocardial circumferential strain and longitudinal strain parameters have prognostic value in various clinical conditions (*13, 14*). Thus, it would be clinically useful to evaluate endocardial strain using a single PET scan, given the association between ischemia and endocardial deformation. We previously developed an original post-processing feature-tracking algorithm for myocardial strain analysis in cardiac magnetic resonance (*15, 16*). We used

the same feature-tracking technique to measure regional myocardial strain during ECG-gated high-resolution cine imaging using ^{13}N-ammonia PET. This study aimed to determine whether feature tracking-derived strain values of PET were associated with myocardial ischemic parameters.

Materials and Methods

Patients

A total of 263 patients, as part of a previous study (January 2017 to January 2019), underwent resting/stressed myocardial ^{13}N-ammonia PET because of known or suspected coronary artery disease (*6*). In this study, we enrolled patients with coronary artery stenosis of more than 50%, diagnosed by coronary computed tomography angiography, from this cohort. Among them, the patients with congenital heart disease, heart failure, or a transplanted heart were excluded. Consequently, 95 patients were retrospectively evaluated. In addition, 10 patients with no coronary stenosis and/or a history of myocardial infarction were randomly selected from the excluded patients as controls. This study was approved by the appropriate institutional review board, and the requirement for written informed consent was waived. None of the patients had cardiovascular risk factors that were retrieved from the patients' medical records at the time of the ^{13}N-ammonia PET.

^{13}N-ammonia PET

After the necessary preparations (*6*), patients were positioned in a three-dimensional PET system (Biograph mCT; Siemens Healthcare, Erlangen, Germany). Repeatedly upgraded Syngo VA30A_HF07 software was used for dose correction (i.e., the difference in residual ^{13}N-ammonia activity between resting and stressed images). Sequential computed tomography scans (120 kV, 20 mAs, and 3-mm slice collimation) were acquired for attenuation correction. Immediately after intravenous administration of ^{13}N-ammonia (approximately 185 MBq, 5 mCi), ECG-gated image acquisition was performed (10 min at 16 frames/cardiac cycle using the parallel list mode) (*17*). After PET myocardial perfusion imaging was performed at rest, the adenosine stress test was performed (0.12 mg/kg/min for 6 min). At 3 min after the

vasodilator administration, ^{13}N-ammonia was infused (approximately 555 MBq, 15 mCi) and myocardial perfusion imaging was performed (Figure 1).

Assessment of myocardial blood flow via MFR

Images were reconstructed using Fourier re-binning and filtered back-projection with a 12-mm three-dimensional Hann window for the ramp filter. The reconstructed images were automatically re-orientated to the 16 short-axis, 8 vertical long-axis, and 8 horizontal long-axis cine images. The pixel size of the cine images was 3.2×3.2 mm, with a 3.0-mm slice thickness. Extraction of mean myocardial and cavity time-activity curves, and generation of polar maps for absolute myocardial blood flow and MFR, were performed using dedicated software (Syngo MI Cardiology; Siemens Healthcare, Erlangen, Germany). The myocardial blood flow was determined based on the LV input time-activity curve and myocardial uptake, using a three-compartment model and a dataset of list mode images that were obtained during the first 2 min of imaging of the list mode data. The MFR values based on a 17-segment model of the right coronary artery (RCA), left anterior descending artery (LAD), and left circumflex coronary artery (LCx) territories were determined from the polar maps, as the ratio of the hyperemic myocardial blood flow to the resting regional myocardial blood flow (*18*). Global MFR was the mean value of MFRs of the RCA, LAD, and LCx territories. Global and regional MFR values <2.0 were considered abnormal (*2*).

Assessment of LV volume and EF

The list mode data from 2 to 10 min were replayed to reconstruct the ECG-gated images. The reconstructed image data with ordered-subsets-expectation-maximization, point-spread function, and time of flight corrections in ^{13}N-ammonia PET, with 21 subsets and four iterations, were transferred to a dedicated software (Syngo MI cardiology, Siemens Healthcare, Erlangen, Germany). The matrix size was 128 x 128, with a slice thickness of 3.0 mm. A three-dimensional cine image of the left ventricle with 16-frames/cardiac cycle was reconstructed (*6*). The quantitative gated single-photon emission computed

tomography algorithm developed by Germano et al. (*19*) was modified for PET to measure the LV volume and obtain the LVEF.

Strain analysis with feature-tracking

The same ECG-gated cine image constructed above was used for strain analysis. The LV regional strain values were semi-automatically calculated using the feature-tracking analysis (*15, 16, 20*). All image processing algorithms for stressed and resting PET were implemented using MATLAB R2020a (version 9.8; Mathworks Inc., Natick, MA), as shown in the Supplementary Movies. The short-axis slices for strain measurements at the base, middle, and apex of the heart were automatically defined as the 3rd, 9th, and 14th slices (among the 16 total images), respectively. Both the vertical long-axis and horizontal long-axis slices for strain measurements were automatically defined as the 4th slice of the 8 vertical long-axis and 8 horizontal long-axis images, respectively. The regional endocardial border was manually defined at end-diastole on the cine images that were displayed in gray color (gamma=1.3) with a standardized uptake value of 10–100% (Figure 2a). Endocardium points were evenly spaced based on the line length (Figure 2b). In this study, 12 points in the short-axis images and 7 points each in the horizontal and vertical long-axis images were set. The points were then automatically tracked during a cardiac cycle, using a local template-matching technique based on normalized correlation coefficient values (Figure 2c). The template images were automatically based on a square area centered on the points: the initial size for the template image was set to 24×24 pixels and search area to 32×32 pixels. However, the template size and search area were updated to ensure successful tracking if the endocardium was not well tracked. The LV endocardial regions were automatically segmented as lines with spline interpolation of the points tracked over a cardiac cycle (Figure 2d). Finally, systolic strain values were calculated from strain curves as the minimum values of the normalized LV regional lengths (Figure 2e). The systolic circumferential strain values of the three short-axis cine images, corresponding to the basal, middle, and apical LV slices, were measured using a previously reported 16-segment model for strain analysis using short-axis images and cardiac magnetic resonance feature-tracking (*21*). Global CS was calculated as the mean value of

systolic circumferential strain for all segments. The regional systolic circumferential strain values for the RCA (segments #3, #4, #9, #10, and #15), LAD (segments #1, #2, #7, #8, #13, and #14), and LCx (segments #5, #6, #11, #12, and #16) territories were calculated as the means of the systolic strain values at the corresponding segments in the 16-segment model. The systolic LS values at the middle LV slice were measured from the anterior and posterior walls on the vertical long-axis cine images, and from the lateral wall and interventricular septum on the horizontal long-axis cine images. Global LS was calculated as the mean of systolic longitudinal strain values from 4 regions on the vertical long-axis and horizontal long-axis images. Systolic longitudinal strain values for the RCA territory, based on the 16-segment model, were obtained from the posterior wall, those for the LAD territory were calculated as the mean of systolic strain values from the anterior wall and interventricular septum, and those for the LCx territory were obtained from the lateral wall.

Intra-observer and inter-observer reproducibility

The intra-observer reproducibility of strain values was evaluated using manually defined endocardial boundaries at end-diastole. Systolic strain values were automatically determined as the minimum values from the 16 frames of each cardiac cycle. A single observer performed all stressed and resting analyses for 30 randomly selected patients and then blindly repeated the analyses at least 1 month later. Inter-observer reproducibility was evaluated based on stressed and resting measurements for the same 30 patients, which were performed by a second observer who was blinded to the clinical and experimental data. The intra-observer and inter-observer reproducibility of the strain measurements was evaluated using Bland–Altman analyses and intraclass correlation coefficients with one-way random or two-way random single measures (intraclass correlation coefficient [1,1] or intraclass correlation coefficient [2,1], respectively). The intraclass correlation coefficient values were defined as excellent (≥0.75), good (0.60–0.74), moderate (0.40–0.59), or poor (≤0.39).

Statistical analysis

All statistical analyses were performed using GraphPad Prism (version 8.1.2 for Mac OS; GraphPad Software, La Jolla, CA). Differences were considered statistically significant at *P*-values of <0.05. The Shapiro–Wilk test was used to evaluate the normality of data distribution and the means and standard deviations were calculated. The global CS and LS values, as well as the systolic circumferential and longitudinal strain values at the RCA, LAD, and LCx territories, of the 3 groups—abnormal global MFR [<2.0], normal global MFR [≥2.0], and control—were compared using the one-way analysis of variance with Tukey or Dunn post hoc analysis. Stressed and resting global systolic strain values, as well as systolic strain values at each territory, were compared using the paired *t*-test or Wilcoxon signed-rank test. Correlations of global systolic strain values (global CS and global LS) with LVEF were analyzed using Spearman correlation coefficients.

Results

Table 1 shows the baseline characteristics and ^{13}N-ammonia PET measurements. Abnormal global MFRs were observed in 39 of 95 patients (41%). All PET-derived scores in patients with abnormal MFRs were lower than those in patients with normal MFRs. There were no differences in the LV end-diastolic and end-systolic volumes in the stressed and resting states between the abnormal and normal MFR groups. Lower stress LVEF was observed in patients with abnormal MFRs than in those with normal MFRs. Abnormal regional MFRs were observed at the RCA (35/95 patients, 37%), LAD (36/95 patients, 38%), and LCx (37/95 patients, 39%). Supplemental Tables 1–3 show in detail the inter-group comparisons of the ^{13}N-ammonia PET measurements according to the regional MFR values.

Figure 3 shows the inter-group and stressed/resting comparisons of the global CS and global LS. Global strains in the stressed state of the abnormal MFR groups were lower than those of the normal MFR and control groups. There were no differences in the resting global strains between the abnormal and normal MFR groups. Global CSs in the stressed state in the abnormal MFR groups were lower than those at the resting state. Global strains in the stressed state in the control groups were higher than those at the resting state. The scatter plots of global strain values and LVEF are shown in Figure 4, and all strain parameters

were significantly correlated with LVEF (all $P<0.01$). Spearman correlation coefficients (confidence intervals) were –0.77 (–0.84, –0.67) for stressed global CS, –0.78 (–0.85, –0.69) for resting global CS, –0.73 (–0.82, –0.62) for stressed global LS, and –0.72 (–0.81, –0.61) for resting global LS. Figure 5 shows the inter-group and stressed/resting comparisons of the regional CS and regional LS. Regional strains in the stressed state of the abnormal MFR groups were lower than those of the control groups in all coronary territories. There were no differences in most of the resting regional strains of the abnormal and normal MFR groups. Regional CSs in the RCA and LCx territories and regional LS in the LAD territory in the stressed state were lower than those in the resting state. CS in the RCA territory and LSs in the RCA and LCx territories in the stressed state in the control groups were higher than those at the resting state. Excellent intra-observer and inter-observer reproducibilities were observed for the feature-tracking technique (Table 2).

Discussion

This study revealed that feature-tracking-derived strain values from a single PET scan could provide a clinically reasonable assessment of regional myocardial motility. Furthermore, the semi-automatic strain measurements via feature-tracking during PET were simple and highly reproducible.

Global and regional strain values in the stressed state were significantly reduced in patients with abnormal MFRs compared with patients with normal MFRs and the control patients. This trend was also observed in the resting strain values. However, the circumferential strain did not significantly decrease in patients with abnormal MFRs. Reduced strain values in the stressed state agree with a previous report on the clinical use of stress echocardiography in ischemic heart disease (*22*); the reduced strain values may be related to transient ischemic dilation in patients with coronary artery disease (*23*) because the LV end-diastole volume in the stressed state is increased by >10% compared to the value in the resting state in patients with coronary artery disease. In the control patients, strain values in the stressed state were either significantly higher or similar to those in the resting state. This myocardial normo-hyperkinesis is consistent with wall motion changes under dobutamine stress echocardiography (*22*). Previously, Eitel et

al. revealed that cardiac magnetic resonance feature-tracking-derived LS provided prognostic information in patients early after reperfused myocardial infarction in comparison to circumferential and radial strains. Also, global LS values provide superior prognostic information over traditional cardiac risk factors, including LVEF (*24*). This is because the endocardial fiber mainly runs in the longitudinal direction, and hence, endocardial ischemia and infarction lead to decreased longitudinal strain. In the present study, there was no significant difference in the reduction of LS and CS in the stressed state in patients with abnormal MFRs. In contrast, in the resting state, the LS tended to be lower than CS in patients with abnormal MFRs. These results suggest that the resting LS is more susceptible to ischemia than CS. Myocardial ischemia evolves from the endocardium to the epicardium, and circumferential strain is greater in the endocardium than in the epicardium (*25*). The simple circle-like LV structure on the SA slice is, therefore, more appropriate to feature-tracking analysis than the HLA and VLA slices. Blurring of myocardial boundaries due to liver accumulation may affect tracking in the inferior wall of the RCA territory. As indicated in Figure 5d, there was no difference in LS in the RCA territory in the stressed state between patients with abnormal and normal MFRs. Thus, the tracking algorithm may need improvement for accurate LS assessment, especially in the inferior wall. We think that the best way to assess regional ischemia is to use LS and CS in a complementary fashion.

Interestingly, the global strain values correlated significantly with LVEF (Figure 3), which is plausible given our previous findings with feature-tracking cardiac magnetic resonance using the same algorithm (*26*). While LVEF is an important clinical marker of the overall LV function, the global strain may be more reliable because it allows detailed analysis of myocardial contraction in the circumferential and longitudinal directions. Global strain assessment using feature-tracking is reportedly effective in predicting the prognosis for various types of heart disease, and is reportedly more effective than EF for this purpose. Although we did not evaluate the relationship between global strain and adverse cardiac events, a combination of global strain and MFR will provide a prognostic value (*27*). Figure 6 shows PET cine imaging and strain polar maps before and after percutaneous coronary intervention for a patient with multi-vessel coronary artery disease. The strain map, as well as the myocardial blood flow and MFR

maps, shows the improvement in regional wall motion after treatment. Thus, a new therapeutic evaluation strategy has been devised by combining regional function and blood flow.

Our strain analysis revealed that strain measurements had excellent inter-observer and intra-observer reproducibilities throughout the cardiac cycle. Nevertheless, PET provides inferior image quality relative to cardiac magnetic resonance, and cardiac magnetic resonance is considered the most appropriate modality for quantitative analysis of the myocardium, owing to its high contrast, spatial resolution, and wide field-of-view. Additionally, the endocardial border was subjectively determined using gray images, although strain measurements using PET feature-tracking are considered equally reproducible relative to cardiac magnetic resonance feature-tracking (*28, 29*). Thus, ^{13}N-ammonia PET images are sufficiently clear for feature-tracking and do not cause reproducibility errors. Furthermore, feature-tracking involves a simple-to-use algorithm and our proposed strain analysis method can automatically calculate the strain for a cardiac cycle using only manual delineation of the regional myocardial wall. Because feature-tracking involves a traditional template-matching technique, the offline tool we used provides regional myocardial strain values within 10 s, which includes the time taken for manually drawing the endocardial borders. Moreover, this analysis can be performed as needed, even after the PET examination, via post-processing strain measurements, and does not require additional image acquisition or additional radioisotope use, which enhances its potential clinical value.

This study had some limitations. We could not compare the patients' PET-derived strain data to that obtained from the same patients using cardiac magnetic resonance or echocardiography. This limitation may raise concerns regarding the accuracy of strain values, although the retrospective study design precluded performing PET and cardiac magnetic resonance examinations for the same patient. Nevertheless, our preliminary results suggest that strain analysis using ^{13}N-ammonia PET has sufficient clinical potential for patients with ischemia. Prospective studies are needed to accumulate further evidence.

In conclusion, we applied myocardial feature-tracking in high-resolution cine imaging in ^{13}N-ammonia PET. The clinically reasonable association between PET-derived strain and MFR suggests that it is

clinically possible to assess blood flow and quantify myocardial motility in ischemia patients using only a single PET examination.

New Knowledge Gained

It is possible to clinically assess blood flow and quantify endocardial motility in ischemia patients using only a single ^{13}N-ammonia positron emission tomography examination.

Acknowledgments

We thank Editage (www.editage.com) for English-language editing.

Disclosures

Masateru Kawakubo has no conflicts of interest to declare.

Michinobu Nagao has no conflicts of interest to declare.

Atsushi Yamamoto has no conflicts of interest to declare.

Risako Nakao has no conflicts of interest to declare.

Yuka Matsuo has no conflicts of interest to declare.

Kenji Fukushim has no conflicts of interest to declare.

Eri Watanabe has no conflicts of interest to declare.

Akiko Sakai has no conflicts of interest to declare.

Masayuki Sasaki has no conflicts of interest to declare.

Shuji Sakai has no conflicts of interest to declare.

Funding

This work was supported by JSPS KAKENHI, Grant Numbers JP20K16729 and JP16K19860.

References

1. Carvajal-Juarez I, Monroy-Gonzalez A, Espinola-Zavaleta N, Meave-Gonzalez A, Alexanderson-Rosas E. PET/CT with 13N-ammonia: PET/CT with 13N-ammonia. Ann Nucl Cardiol 2019;5:63-8.
2. Fiechter M, Ghadri JR, Gebhard C, Fuchs TA, Pazhenkottil AP, Nkoulou RN, et al. Diagnostic value of 13N-ammonia myocardial perfusion PET: Added value of myocardial flow reserve. J Nucl Med 2012;53:1230-4.
3. Giubbini R, Peli A, Milan E, Sciagrà R, Camoni L, Albano D, et al. Comparison between the summed difference score and myocardial blood flow measured by 13N-ammonia. J Nucl Cardiol 2018;2:1621-8.
4. Fathala A, Aboulkheir M, Shoukri MM, Alsergani H. Diagnostic accuracy of 13 N-ammonia myocardial perfusion imaging with PET-CT in the detection of coronary artery disease. Cardiovasc Diagn Ther 2019;9:35-42.
5. Herzog BA, Husmann L, Valenta I, Gaemperli O, Siegrist PT, Tay FM, et al. Long-term prognostic value of 13N-ammonia myocardial perfusion positron emission tomography. Added value of coronary flow reserve. J Am Coll Cardiol 2009;54:150-6.
6. Nakao R, Nagao M, Yamamoto A, Fukushima K, Watanabe E, Sakai S, et al. Papillary muscle ischemia on high-resolution cine imaging of nitrogen-13 ammonia positron emission tomography: Association with myocardial flow reserve and prognosis in coronary artery disease. J Nucl Cardiol 2020; doi:10.1007/s12350-020-02231-z.
7. Khorsand A, Graf S, Eidherr H, Wadsak W, Kletter K, Sochor H, et al. Gated cardiac 13N-NH3 PET for assessment of left ventricular volumes, mass, and ejection fraction: comparison with electrocardiography-gated 18F-FDG PET. J Nucl Med 2005;46:2009-13.
8. Nagao M, Hatakenaka M, Matsuo Y, Kamitani T, Higuchi K, Shikata F, et al. Subendocardial contractile impairment in chronic ischemic myocardium: Assessment by strain analysis of 3T tagged CMR. J Cardiovasc Magn Reson 2012;14:14.

9. Kido T, Nagao M, Kido T, Kurata A, Miyagawa M, Ogimoto A, et al. Stress/rest circumferential strain in non-ischemia, ischemia, and infarction: Quantification by 3 tesla tagged magnetic resonance imaging. Circ J 2013;77:1235-41.
10. Driss AB, Lepage BDC, Sfaxi A, Hakim M, Elhadad S, Tabet JY, et al. Strain predicts left ventricular functional recovery after acute myocardial infarction with systolic dysfunction. Int J Cardiol 2020;307:1-7.
11. Stathogiannis K, Mor-Avi V, Rashedi N, Lang RM, Patel AR. Regional myocardial strain by cardiac magnetic resonance feature tracking for detection of scar in ischemic heart disease. Magn Reson Imaging 2020;68:190-6.
12. Berry C, Mangion K, Pathan F. Spotlight on strain following myocardial infarction. JACC Cardiovasc Imaging 2018;11:1445-7.
13. Reindl M, Tiller C, Holzknecht M, Lechner I, Beck A, Plappert D, et al. Prognostic implications of global longitudinal strain by feature-tracking cardiac magnetic resonance in ST-elevation myocardial infarction. Circ Cardiovasc Imaging 2019;12:e009404.
14. Mordi I, Bezerra H, Carrick D, Tzemos N. The combined incremental prognostic value of LVEF, late gadolinium enhancement, and global circumferential strain assessed by CMR. JACC Cardiovasc Imaging 2015;8:540-9.
15. Kawakubo M, Yamasaki Y, Kamitani T, Sagiyama K, Matsuura Y, Hino T, et al. Clinical usefulness of right ventricular 3D area strain in the assessment of treatment effects of balloon pulmonary angioplasty in chronic thromboembolic pulmonary hypertension: comparison with 2D feature-tracking MRI. Eur Radiol 2019;29:4583-92.
16. Kawakubo M, Nagao M, Ishizaki U, Shiina Y, Inai K, Yamasaki Y, et al. Feature-tracking MRI fractal analysis of right ventricular remodeling in adults with congenitally corrected transposition of the great arteries. Radiol Cardiothorac Imaging 2019;1:e190026.
17. Dilsizian V, Bacharach SL, Beanlands RS, Bergmann SR, Delbeke D, Dorbala S, et al. ASNC imaging guidelines/SNMMI procedure standard for positron emission tomography (PET) nuclear

cardiology procedures. J Nucl Cardiol 2016;23:1187-26.

18. Cerqueira MD, Weissman, NJ, Dilsizian V, Jacobs AK, Kaul S, Laskey WK, et al. Standardized myocardial segmentation and nomenclature for tomographic imaging of the heart. J Cardiovasc Magn Reson 2002;4:203-10.
19. Germano G, Erel J, Kiat H, Kavanagh PB, Berman DS. Quantitative LVEF and qualitative regional function from gated thallium-201 perfusion SPECT. J Nucl Med 1997;38:749-54.
20. Yamasaki Y, Abe K, Kamitani T, Hosokawa K, Kawakubo M, Sagiyama K, et al. Balloon pulmonary angioplasty improves right atrial reservoir and conduit functions in chronic thromboembolic pulmonary hypertension. Eur Heart J Cardiovasc Imaging 2020;21:855-62.
21. Mangion K, Burke NMM, McComb C, Carrick D, Woodward R, Berry C. Feature-tracking myocardial strain in healthy adults- a magnetic resonance study at 3.0 tesla. Sci Rep 2019;9:3239.
22. Sicari R, Cortigiani L. The clinical use of stress echocardiography in ischemic heart disease. Cardiovasc Ultrasound 2017;15:7.
23. Weiss AT, Berman DS, Lew AS, Nielsen J, Potkin B, Swan HJ, et al. Transient ischemic dilation of the left ventricle on stress thallium-201 scintigraphy: A marker of severe and extensive coronary artery disease. J Am Coll Cardiol 1987;9:752-9.
24. Eitel I, Stiermaier T, Lange T, Rommel KP, Koschalka A, Kowallick JT, et al. Cardiac magnetic resonance myocardial feature tracking for optimized prediction of cardiovascular events following myocardial infarction. JACC Cardiovasc Imaging 2018;11:1433-44.
25. Cheng A, Langer F, Rodriguez F, Criscione JC, Daughters GT, Miller DC, et al. Transmural cardiac strains in the lateral wall of the ovine left ventricle. Am J Physiol Hear Circ Physiol 2005;288:1546-56.
26. Kawakubo M, Arai H, Nagao M, Yamasaki Y, Sanui K, Nishimura H, et al. Global left ventricular area strain using standard two-dimensional cine magnetic resonance imaging with inter-slice interpolation. Cardiovasc Imaging Asia 2018;2:187-93.
27. Ishizaki U, Nagao M, Shiina Y, Inai K, Mori H, Takahashi T, et al. Global strain and dyssynchrony

of the single ventricle predict adverse cardiac events after the Fontan procedure: Analysis using feature-tracking cine magnetic resonance imaging. J Cardiol 2019;73:163-70.

28. Schmidt B, Dick A, Treutlein M, Schiller P, Bunck AC, Maintz D, et al. Intra- and inter-observer reproducibility of global and regional magnetic resonance feature tracking derived strain parameters of the left and right ventricle. Eur J Radiol 2017;89:97-105.
29. Alfakih K, Plein S, Thiele H, Jones T, Ridgway JP, Sivananthan MU. Normal human left and right ventricular dimensions for MRI as assessed by turbo gradient echo and steady-state free precession imaging sequences. J Magn Reson Imaging 2003;17:323-9.

FIGURE LEGENDS

Fig. 1 Resting and adenosine stress protocols for ^{13}N-ammonia PET

A low-dose fast helical (1.5-s) computed tomography scan was performed for attenuation correction. Next, ^{13}N-ammonia (185 MBq) was administered intravenously, and electrocardiography-gated acquisition was performed (10 min at 16 frames/cardiac cycle using a parallel list mode). After the resting PET scan, an adenosine stress test was performed (0.12 mg/kg/min for 6 min). Then, ^{13}N-ammonia (555 MBq) was infused at 3 min after completion of the vasodilator infusion, and the stress PET scan was performed using the same acquisition parameters.

PET, positron emission tomography

Fig. 2 Semi-automatic strain analysis with feature-tracking

(a) The regional endocardial border is manually defined at the end of the diastole frame (left: short-axis, middle: horizontal long-axis, right: vertical long-axis). (b) Endocardium points are automatically and evenly set based on the line length. (c) The points are automatically tracked during a cardiac cycle using a local template-matching technique. (d) The endocardial regions are automatically segmented as lines with spline interpolation of points tracked during a cardiac cycle. Systolic strain is calculated from the strain curves as the minimum values of the normalized regional lengths.

Fig. 3 Global systolic strain values according to global MFR status

(a) Global circumferential strain values for patients with abnormal global myocardial flow reserves (purple/dark purple, <2.0) and normal global myocardial flow reserves (red/dark red, ≥2.0), and in control patients (cyan/dark cyan). (b) Global longitudinal strain values for patients with abnormal global myocardial flow reserves (purple/dark purple, <2.0) and normal global myocardial flow reserves (red/dark red, ≥2.0), and in control patients (cyan/dark cyan).

**p<0.01, *p<0.05. MFR, myocardial flow reserve

Fig. 4 Correlations between global strains and LVEFs

Scatter plots show the correlations between global strain and LVEF. Plots in the upper row and lower row indicate the values in the stressed and resting states, respectively. Plots in the left and right columns indicate the correlations of LVEF with circumferential and longitudinal strains, respectively.

LVEF, left ventricular ejection fraction

Fig. 5 Regional systolic strain values according to regional MFR status

Strain values for patients with abnormal myocardial flow reserves (purple/dark purple, <2.0) and normal myocardial flow reserves (red/dark red, ≥2.0), and in control patients (cyan/dark cyan): the upper low indicates the circumferential strain values of the right coronary artery territory (a), left anterior descending artery territory (b), and left circumflex coronary artery territory (c), and the lower low indicates the longitudinal strain values of the right coronary artery territory (d), left anterior descending artery territory (e), and left circumflex coronary artery territory (f).

***p*<0.01, **p*<0.05. MFR, myocardial flow reserve

Fig. 6 Circumferential strain polar maps at stress (left) and ^{13}N-ammonia PET cine images (right) for a woman in her 60s with 90% stenosis at the proximal LAD, 50% stenosis at the proximal RCA, and 50% stenosis at the diagonal branch

Before (upper row) and after (lower row) percutaneous coronary intervention. The cold color of the strain map indicates a decrease in strain, while the warm color indicates an increase. After percutaneous coronary intervention, there is a marked improvement in strain reduction over a wide area of the apex to anteroseptal wall, and the cine images show improvement of blood flow in the anteroseptal wall and reduction of the left ventricular cavity.

TABLE 1 Baseline patient characteristics and ^{13}N-ammonia PET measurements

Characteristics	Patients			*P*-value	Control
	All	Global MFR<2.0	Global MFR≥2.0		
Number	95	39	56		10
Age (years)	68±11	71±10	65±11	<0.05	41±15
Male/female	62/33	22/17	40/16		6/4
Cardiovascular risk factors					
Hypertension	69 (73%)	29 (74%)	40 (71%)		0 (0%)
Dyslipidemia	68 (72%)	23 (60%)	45 (80%)		0 (0%)
Diabetes mellitus	44 (46%)	18 (46%)	26 (46%)		0 (0%)
Smoking	42 (44%)	15 (38%)	27 (48%)		0 (0%)
Family history	22 (23%)	8 (21%)	14 (25%)		0 (0%)
Clinical history of coronary artery disease					
Myocardial infarction	14 (15%)	11 (28%)	3 (5%)		0 (0%)
Percutaneous coronary intervention	21 (22%)	11 (28%)	10 (18%)		0 (0%)
Coronary artery bypass grafting	8 (8%)	3 (8%)	5 (9%)		0 (0%)
Ammonia PET measurements					
Summed stress score	5.7±7.1	8.6± .3	3.6±5.3	<0.01	1.5±3.3
Summed resting score	1.8±3.4	2.7±4.2	1.1±2.5	<0.01	0.5±1.2
Summed difference score	3.9±5.8	5.9±7.5	2.5±3.7	<0.01	1.0±2.2
Stressed myocardial blood flow (mL/g/min)	2.07±0.65	1.62±0.55	2.39±0.52	<0.01	2.43±1.00
Resting myocardial blood flow (mL/g/min)	0.98±0.25	1.05±0.29	0.92±0.22	0.03	1.06±0.28
Global MFR	2.2±0.7	1.5±0.4	2.6±0.5	<0.01	2.2±0.6
RCA MFR	2.3±0.8	1.5±0.5	2.7±0.6	<0.01	2.3±0.6

LAD MFR	2.2±0.7	1.6±0.5	2.6±0.6	<0.01	2.3±0.6
LCx MFR	2.2±0.7	1.6±0.4	2.6±0.6	<0.01	2.2±0.6
Resting LVEDV (mL)	88±28	90±34	86±24	0.79	71±15
Resting LVESV (mL)	30±22	36±28	25±15	0.14	17±5
Resting LVEF (%)	70±12	66±15	72±10	<0.05	76±5
Stress LVEDV (mL)	101±28	103±33	100±26	0.84	76±15
Stress LVESV (mL)	34±22	43±28	31±17	0.06	17±5
Stress LVEF (%)	67±12	62±16	71±9	<0.01	78±4

MFR, myocardial flow reserve; RCA, right coronary artery; LAD, left anterior descending artery; LCx, left circumflex artery; LV, left ventricular; EDV, end-diastole volume; ESV, end-systole volume; EF, ejection fraction.

TABLE 2 Reproducibility of strain analyses

Parameter		Intra-observer reproducibility			Inter-observer reproducibility		
		Bias (LOA)	SDD	ICC (95% CI)	Bias (LOA)	SDD	ICC (95% CI)
Stress							
Global	CS	−0.7 (−3.5, 2.0)	1.4	0.98 (0.92–0.99)	−0.1 (−2.7, 2.5)	1.3	0.98 (0.93–1.00)
	LS	0.4 (−1.6, 2.3)	1.0	0.95 (0.82–0.99)	3.2 (−0.2, 6.7)	1.7	0.97 (0.89–0.99)
RCA	CS	−0.2 (−6.6, 6.1)	3.2	0.97 (0.96–0.98)	−0.1 (−5.3, 5.0)	2.6	0.96 (0.84–0.99)
	LS	0.8 (−4.0, 5.6)	2.5	0.985(0.83–0.99)	4.9 (1.5, 8.4)	1.8	0.97 (0.90–0.99)
LAD	CS	−0.7 (−4.8, 3.4)	2.1	0.97 (0.88–0.99)	0.5 (−4.1, 5.1)	2.4	0.96 (0.83–0.99)
	LS	0.3 (−1.6, 2.2)	1.0	0.99 (0.97–1.00)	2.5 (−2.2, 7.2)	2.4	0.94 (0.79–0.99)
LCx	CS	−0.5 (−6.9, 5.9)	3.3	0.91 (0.68–0.98)	−0.8 (−6.2, 4.6)	2.8	0.91 (0.68–0.98)
	LS	−0.0 (−1.9, 1.9)	0.98	0.99 (0.97–1.00)	3.0 (−1.1, 7.2)	2.1	0.96 (0.85–0.99)
Resting							
Global	CS	−0.7 (−3.5, 2.0)	1.4	0.99 (0.95–1.00)	−0.1 (−2.7, 2.5)	1.3	0.98 (0.93–1.00)

RCA	CS	0.1 (–5.2, 5.5)	2.7	0.96 (0.85–0.99)	1.0 (–3.8, 5.7)	2.4	0.96 (0.86–0.99)
	LS	0.0 (1.9, 1.9)	1.0	0.99 (0.97–1.00)	3.0 (–1.1, 7.2)	2.1	0.96 (0.85–0.99)
LAD	CS	−0.1 (–5.2, 5.0)	2.6	0.96 (0.87–0.99)	–0.2 (–3.9, 3.6)	1.9	0.98 (0.92–0.99)
	LS	0.2 (–2.2, 2.6)	1.2	0.99 (0.96–1.00)	1.9 (–3.0, 6.9)	2.5	0.94 (0.79–0.99)
LCx	CS	–1.5 (–8.2, 5.1)	3.4	0.94 (0.78–0.98)	0.3 (–7.4, 8.0)	3.9	0.92 (0.70–0.98)
	LS	–0.0 (–1.9, 1.9)	1.0	0.99 (0.97–1.00)	3.0 (–1.1, 7.2)	2.1	0.96 (0.85–0.99)

RCA, right coronary artery; LAD, left anterior descending artery; LCx, left circumflex artery; CS; circumferential strain, LS; longitudinal strain, LOA, limit of agreement; SDD, standard deviation of the difference; ICC, intraclass correlation coefficient; CI, confidence interval.

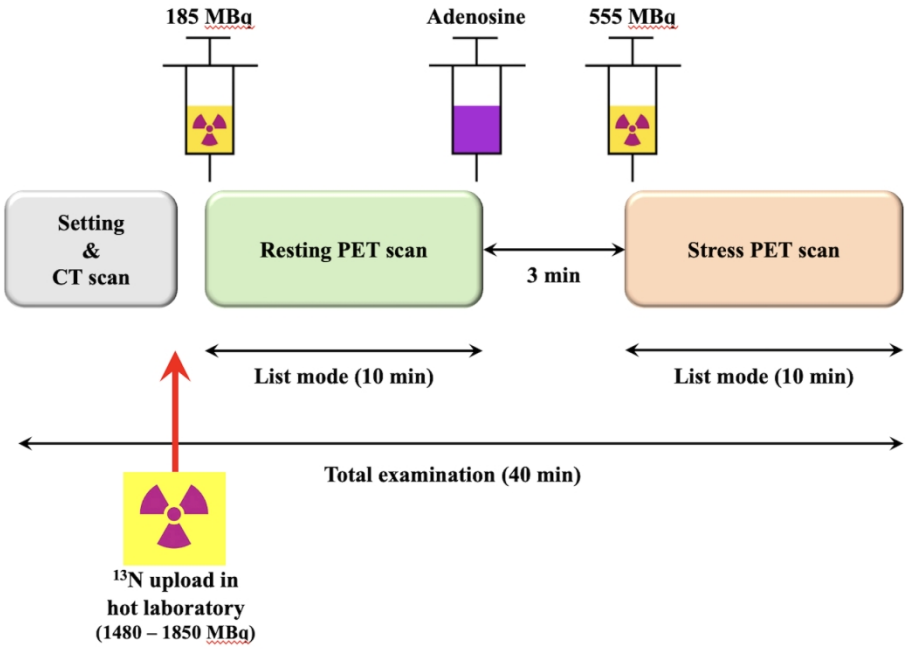

Resting and adenosine stress protocols for ^{13}N-ammonia positron emission tomography A low-dose fast helical (1.5-s) computed tomography scan was performed for attenuation correction. Next, ^{13}N-ammonia (185 MBq) was administered intravenously, and electrocardiography-gated acquisition was performed (10 min at 16 frames/cardiac cycle using a parallel list mode). After the resting PET scan, an adenosine stress test was performed (0.12 mg/kg/min for 6 min). Then, ^{13}N-ammonia (555 MBq) was infused at 3 min after completion of the vasodilator infusion, and the stress PET scan was performed using the same acquisition parameters.PET, positron emission tomography

84x59mm (600 x 600 DPI)

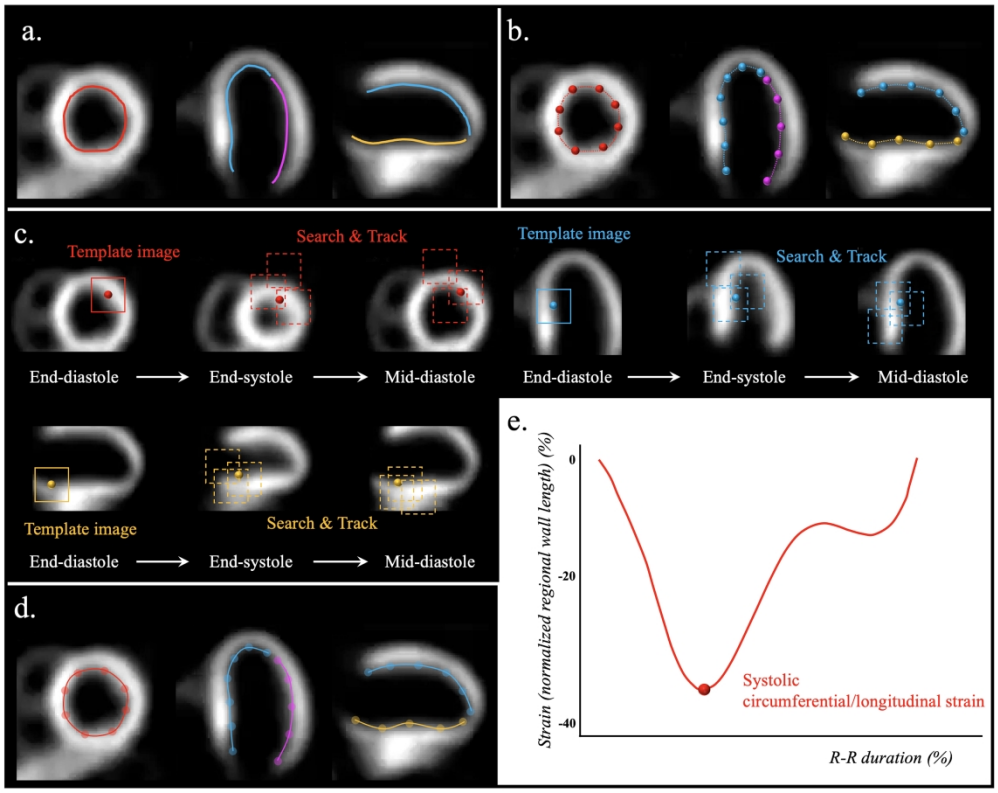

Semi-automatic strain analysis with feature-tracking

(a) The regional endocardial border is manually defined at the end of the diastole frame (left: short-axis, middle: horizontal long-axis, right: vertical long-axis). (b) Endocardium points are automatically and evenly set based on the line length. (c) The points are automatically tracked during a cardiac cycle using a local template-matching technique. (d) The endocardial regions are automatically segmented as lines with spline interpolation of points tracked during a cardiac cycle. Systolic strain is calculated from the strain curves as the minimum values of the normalized regional lengths.

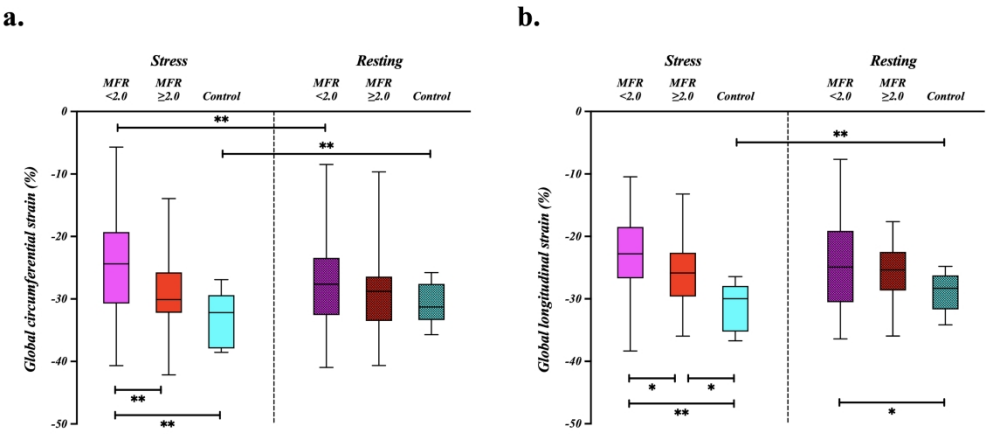

Global systolic strain values according to global MFR status

(a) Global circumferential strain values for patients with abnormal global myocardial flow reserves (purple/dark purple, <2.0) and normal global myocardial flow reserves (red/dark red, ≥2.0), and in control patients (cyan/dark cyan). (b) Global longitudinal strain values for patients with abnormal global myocardial flow reserves (purple/dark purple, <2.0) and normal global myocardial flow reserves (red/dark red, ≥2.0), and in control patients (cyan/dark cyan).

$^{**}p<0.01$, $^{*}p<0.05$. MFR, myocardial flow reserve

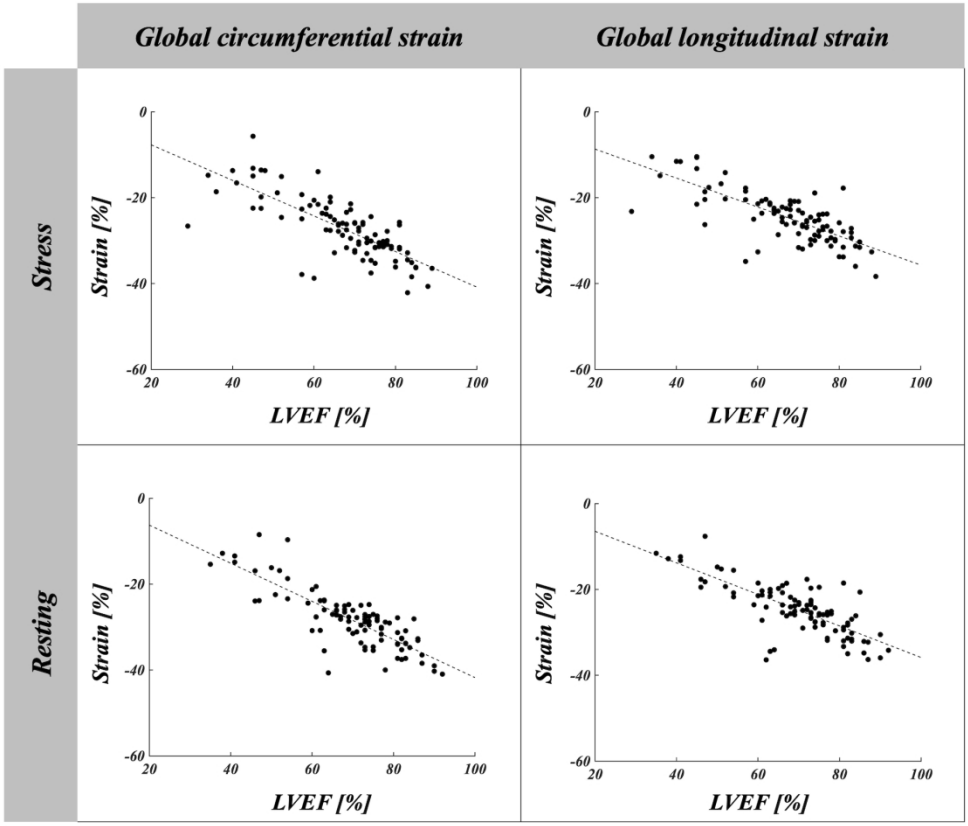

Correlations between global strains and LVEFs Scatter plots show the correlations between global strain and LVEF. Plots in the upper row and lower row indicate the values in the stressed and resting states, respectively. Plots in the left and right columns indicate the correlations of LVEF with circumferential and longitudinal strains, respectively.LVEF, left ventricular ejection fraction

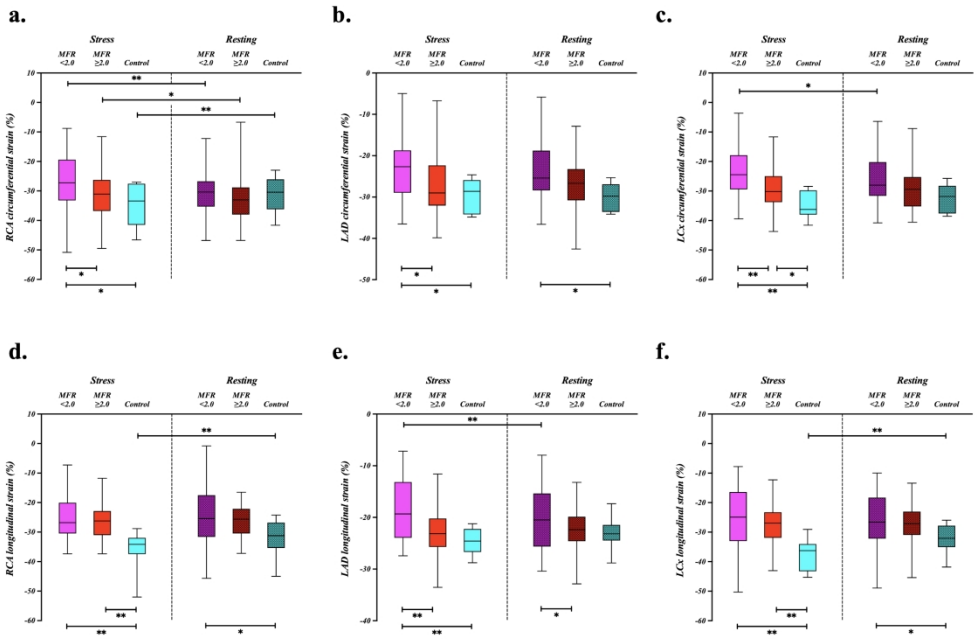

Regional systolic strain values according to regional MFR status

Strain values for patients with abnormal myocardial flow reserves (purple/dark purple, <2.0) and normal myocardial flow reserves (red/dark red, ≥2.0), and in control patients (cyan/dark cyan): the upper low indicates the circumferential strain values of the right coronary artery territory (a), left anterior descending artery territory (b), and left circumflex coronary artery territory (c), and the lower low indicates the longitudinal strain values of the right coronary artery territory (d), left anterior descending artery territory (e), and left circumflex coronary artery territory (f).

$^{**}p<0.01$, $^{*}p<0.05$. MFR, myocardial flow reserve

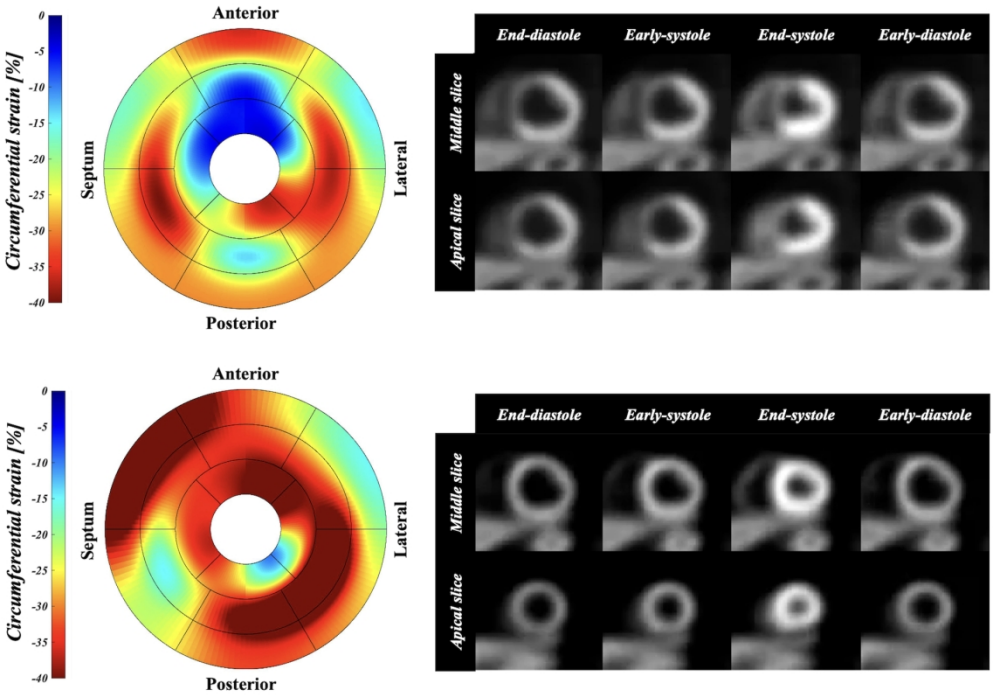

Circumferential strain polar maps at stress (left) and 13N-ammonia PET cine images (right) for a woman in her 60s with 90% stenosis at the proximal LAD, 50% stenosis at the proximal RCA, and 50% stenosis at the diagonal branch

Before (upper row) and after (lower row) percutaneous coronary intervention. The cold color of the strain map indicates a decrease in strain, while the warm color indicates an increase. After percutaneous coronary intervention, there is a marked improvement in strain reduction over a wide area of the apex to anteroseptal wall, and the cine images show improvement of blood flow in the anteroseptal wall and reduction of the left ventricular cavity.

84x61mm (600 x 600 DPI)

Supplementary Movies

Supplementary Movie 1

Short-axis: Calculation of the short-axis regional circumferential strain at the middle ventricle and the tracked points during a cardiac cycle. Cyan solid and dotted lines indicate segments 7 and 8 of the left ventricle, yellow solid and dotted lines indicate segments 9 and 10, and magenta solid and dotted lines indicate segments 11 and 12. This algorithm can be made available by contacting our research team (contact: k-mstr@hs.med.kyushu-u.ac.jp).

Supplementary Movie 2

Horizontal long-axis: Calculation of the horizontal long-axis regional strain at the middle ventricle and the tracked points during a cardiac cycle. The magenta solid line indicates the longitudinal strain curve for a cardiac cycle. This algorithm can be made available by contacting our research team (contact: k-mstr@hs.med.kyushu-u.ac.jp).

Supplementary Movie 3

Vertical long-axis: Calculation of vertical long-axis regional strain at the middle ventricle and the tracked points during a cardiac cycle. The magenta solid line indicates the longitudinal strain curve for a cardiac cycle. This algorithm can be made available by contacting our research team (contact: k-mstr@hs.med.kyushu-u.ac.jp).